

Active Sensing of Knee Osteoarthritis Progression with Reinforcement Learning

Khanh **Nguyen**, Huy Hoang **Nguyen**, Egor **Panfilov**, Aleksei **Tiulpin***

Research Unit of Health Sciences and Technology, University of Oulu, Oulu, Finland

ABSTRACT

Osteoarthritis (OA) is the most common musculoskeletal disease, which has no cure. Knee OA (KOA) is one of the highest causes of disability worldwide, and it costs billions of United States dollars to the global economy. Prediction of KOA progression has been of high interest to the research community for years, as it can advance treatment development through more efficient clinical trials and improve patient outcomes through more efficient healthcare utilization. Existing approaches for predicting KOA, however, are predominantly static, i.e. consider data from a single time point to predict progression many years into the future, and knee level, i.e. consider progression in a single joint only. Due to these and related reasons, these methods fail to deliver the level of predictive performance, which is sufficient to result in cost savings and better patient outcomes. Collecting extensive data from all patients on a regular basis could address the issue, but it is limited by the high cost at a population level. In this work, we propose to go beyond static prediction models in OA, and bring a novel Active Sensing (AS) approach, designed to dynamically follow up patients with the objective of maximizing the number of informative data acquisitions, while minimizing their total cost over a period of time. Our approach is based on Reinforcement Learning (RL), and it leverages a novel reward function designed specifically for AS of disease progression in more than one part of the human body. Our method relies on multi-modal Deep Learning and requires no human input at test time. Throughout an exhaustive experimental evaluation, we show that using RL can provide a higher monetary benefit when compared to state-of-the-art baselines. Finally, our work introduces a novel AS benchmark for RL in medicine, which we make publicly available at <https://github.com/Oulu-IMEDS/OACostSensitivityRL>.

Keywords: Active Sensing, Reinforcement Learning, Deep Learning, Knee Osteoarthritis

1. Introduction

Osteoarthritis (OA) is a degenerative joint disorder that affects primarily the knee cartilage, and results in its gradual loss and subsequent damage to the joint (Primorac et al., 2020). Knee OA (KOA), the most frequent type of OA, is studied in this work. Common symptoms of KOA include pain, stiffness, and reduced joint flexibility, all of which significantly impact an individual's quality of life. As the condition progresses, the symptoms often worsen, decreasing mobility and potentially leading to disability (McAlindon et al., 1993).

To date, there are no effective treatments that can prevent long-term disability and permanent joint damage in KOA (Hafez et al., 2014). At the latest stages of KOA, a costly and highly invasive intervention, such as total knee replacement (TKR), is delivered to improve the patient's health and well-being. A TKR surgery may cost up to \$50,000 for each

patient (Price et al., 2018; Evans, 2018; Phillips et al., 2019), and TKR reportedly yields unsatisfactory results in 15-20% of cases (Marsh et al., 2022; Bourne et al., 2010; Price et al., 2018). Due to rapid population aging, TKR gradually becomes a financial burden not only for individuals (Kjellberg and Kehlet, 2016) but also for the healthcare system (Gandhi et al., 2023). Therefore, KOA in general, requires the next-generation disease-modifying drugs (DMOADs) (Oo et al., 2018; Rodriguez-Merchan, 2023). Such therapies should aim at slowing down the disease progression, thereby delaying the need for TKR (Latourte et al., 2020; Cho et al., 2021).

While the research community has been working on KOA DMOADs for a number of years (Pfizer, 2010; Hunter, 2011), no drugs have yet been found effective and approved by the regulatory bodies (Rodriguez-Merchan, 2023). One of the challenges in developing DMOADs for KOA is the long patient follow-up time in clinical trials (Latourte et al., 2020). KOA is often a slowly progressing disease with an unknown

*Corresponding author:

e-mail: aleksei.tiulpin@oulu.fi (Aleksei Tiulpin)

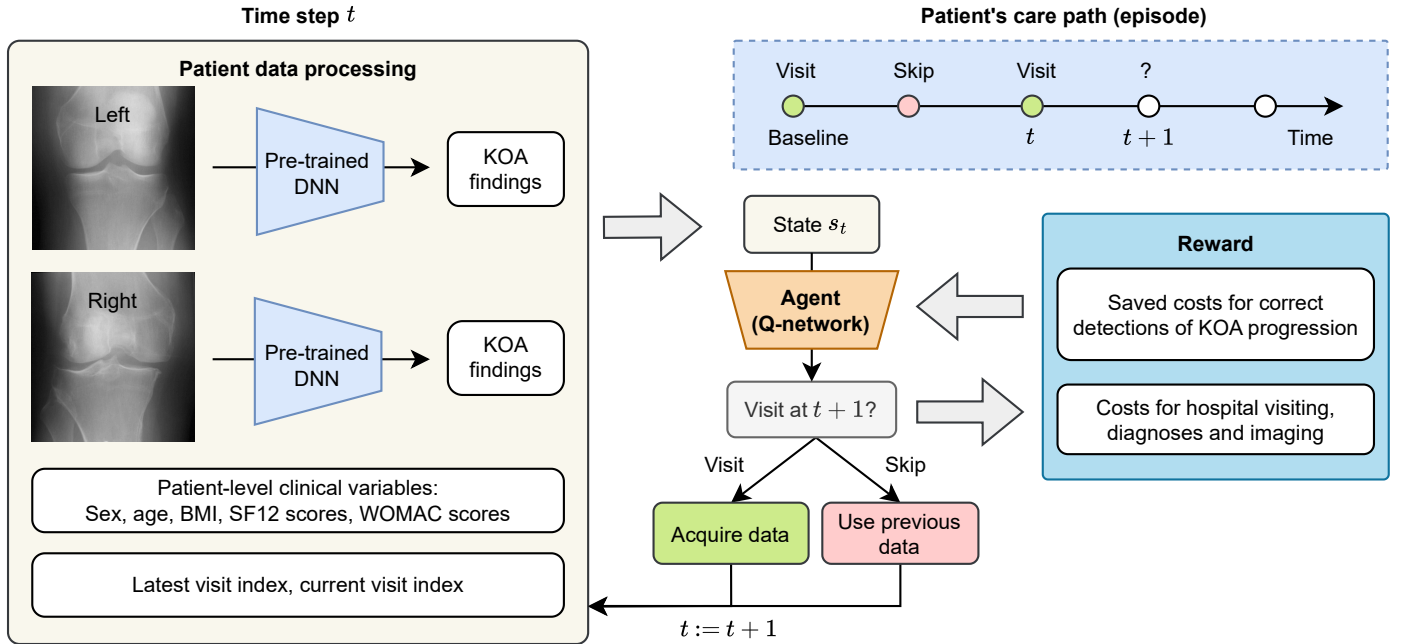


Fig. 1: The workflow of our active sensing method, is represented as decision-making under uncertainty. The state at each time point is associated with the data acquired at the latest patient visit. A reward function is designed to maximize the efficiency of hospital visits by taking into account radiographic changes and hospital visit costs. The actions set contains two actions – follow-up at time t or skip.

etiology (Driban et al., 2020). Thus, many subjects recruited to KOA trials and cohorts do not develop the disease at all and some develop only early signs of the disease by the end of a study. Hence, adaptive methods for data acquisition in modern clinical trials (Spreafico et al., 2021; Cuzick, 2023) are becoming instrumental to providing better, and more cost-efficient patient monitoring compared to routine scheduling and randomized participant selection (Wu and Suen, 2022; Yala et al., 2022).

Despite recent advancements in the field of KOA progression prediction (Halilaj et al., 2018; McCabe et al., 2022; Tiulpin et al., 2019a; Nguyen et al., 2022, 2023), translation of existing models into real-world applications is challenging for several reasons. Firstly, the financial downstream impact of the disease progression models is hard to assess during the model development phase. As such, the current models do not account for *follow-up costs* and potential *future expenses* associated with structural KOA progression when they estimate if a person will develop KOA in the future. Secondly, the existing models, e.g. (Tiulpin et al., 2019a, 2022; Nguyen et al., 2023; Hirvasniemi et al., 2023; Hu et al., 2022; Panfilov et al., 2022, 2023) largely focus only on the knee-level

progression events and overlook KOA’s broader patient-level context, where progression may happen concurrently in both knees. Thirdly, OA severity may increase multiple times during the study time, and there are uncertain future factors that may alter the disease course (e.g. future injuries). Therefore, long-horizon prediction is hard, and one must rethink the paradigm of predicting OA progression.

Active Sensing (AS) (Yu et al., 2009) addresses the question of *when* to follow up patient and with *what tools* or modalities an examination has to be conducted. In the case of KOA, one would want an AS policy to minimize the follow-up costs while maximizing the chances of capturing patient-level progression. Solving such a problem, however, is challenging for a naïve supervised learning (SL) approach, as AS involves making predictions to acquire new data, which in turn informs further predictions, leading to a continuous cycle of adaptive data collection. This is a hardly differentiable problem of decision-making under uncertainty, which can be solved using e.g. Reinforcement Learning (RL) (Sutton and Barto, 2018).

In this work, we develop an AS methodology for KOA using RL. We utilize RL to make sequential decisions based on the

interactions between a decision-making agent and an environment simulating a clinical trial or another setting where patients need to be observed on an interval basis for a prolonged period of time. The overview of our method is depicted in [Figure 1](#), and the specific contributions of our work are:

- We introduce a formal framework for personalized AS into the KOA domain to enhance the efficiency of clinical trials.
- We propose to dynamically model and predict KOA progression at the patient level.
- We employ an RL-based model to derive a personalized patient follow-up schedule that is being refined dynamically, taking into account costs and data utility from a clinical perspective.
- We propose a new reward function, designed specifically for AS of structural KOA degeneration.
- We set up a novel AS baseline for the field of OA, particularly, KOA. We openly release the code and a newly developed RL environment to foster the development of new methods and approaches.

2. Methodology

2.1. Problem definition

We consider a set of participants in a longitudinal observational setting and assume that all of them have been examined at the baseline, corresponding to $t = 0$. If a subject visits the hospital at time t , we observe a state – a set of *multi-modal data* consisting of clinical variables and imaging data, denoted by s_t , which is needed for KOA diagnosis at t . This examination incurs a certain acquisition cost (visit cost), which we denote by λ .

Our objective is to make optimal, w.r.t. both costs and outcomes over a defined time interval T , *sequential decisions* to refer each subject for an examination, to capture the disease progression using the acquired multi-modal data. We illustrated the decision-making process in [Figure 2](#). Specifically,

for each subject, at time point $t \in \{0, \dots, T - 1\}$, we predict whether that subject should be examined at the next time point $t + 1$. The referral for an examination is considered successful if the disease has progressed between t and $t + 1$. We formalize this as the following optimization problem:

$$\{a_0^*, \dots, a_{T-1}^*\} = \underset{\{a_0, \dots, a_{T-1}\}}{\operatorname{argmin}} \frac{1}{T} \sum_{t=0}^{T-1} J(s_t, a_t, \{y_i\}_{i=1}^T, \lambda), \quad (1)$$

where action $a_t \in \{0, 1\}$ indicates whether to issue a referral for a visit at time-point $t + 1$. We assume that the value of the objective J depends on the actions a_t , states s_t , and patient-level disease trajectory $\{y_i\}_{i=1}^T$ (in this study, KOA). The cost of data acquisition λ is treated as a hyper-parameter. We also use λ as a basic cost unit multiplier when defining the costs of undetected disease progression.

The optimization problem defined in (1) is the problem of learning to make sequential decisions under uncertainty. We further define this problem through the prism of Markov Decision Processes (MDP) and RL.

2.2. Reinforcement Learning

Markov Decision Process. An MDP is defined as a tuple $(\mathbf{S}, \mathbf{A}, P, R, \gamma)$, where \mathbf{S} is a set of states, \mathbf{A} is a set of actions. $P: \mathbf{S} \times \mathbf{S} \times \mathbf{A} \rightarrow [0, 1]$ indicates transition probabilities between states. Finally, $R: \mathbf{S} \times \mathbf{A} \rightarrow \mathbb{R}$ represents a set of rewards associated with state-action pairs and $\gamma \in [0, 1]$ is the discounting factor ([Sutton and Barto, 2018](#)). The decision-making policy of an agent is defined by $\pi: \mathbf{A} \times \mathbf{S} \rightarrow [0, 1]$.

In the MDP framework, the sequential decision-making process unfolds as follows ([Sutton and Barto, 2018](#)). At a time step $t \in \mathbb{N}$, the environment (a “world” in which the agent exists and makes actions) yields a state $s_t \in \mathbf{S}$ that is observed by the agent. The agent then responds with an action $a_t \in \mathbf{A}$ following the policy $\pi(a_t | s_t)$. The policy assigns a probability to the event associated with selecting action a_t at a state s_t . Subsequently, the environment provides a reward $r_t = R(s_t, a_t)$ to the agent for taking the action a_t . The process then repeats until the horizon is reached (i.e. $t = T$). We use the term *experiences* to refer to a collection of states s_t , next states s_{t+1} , actions a_t , and rewards r_t .

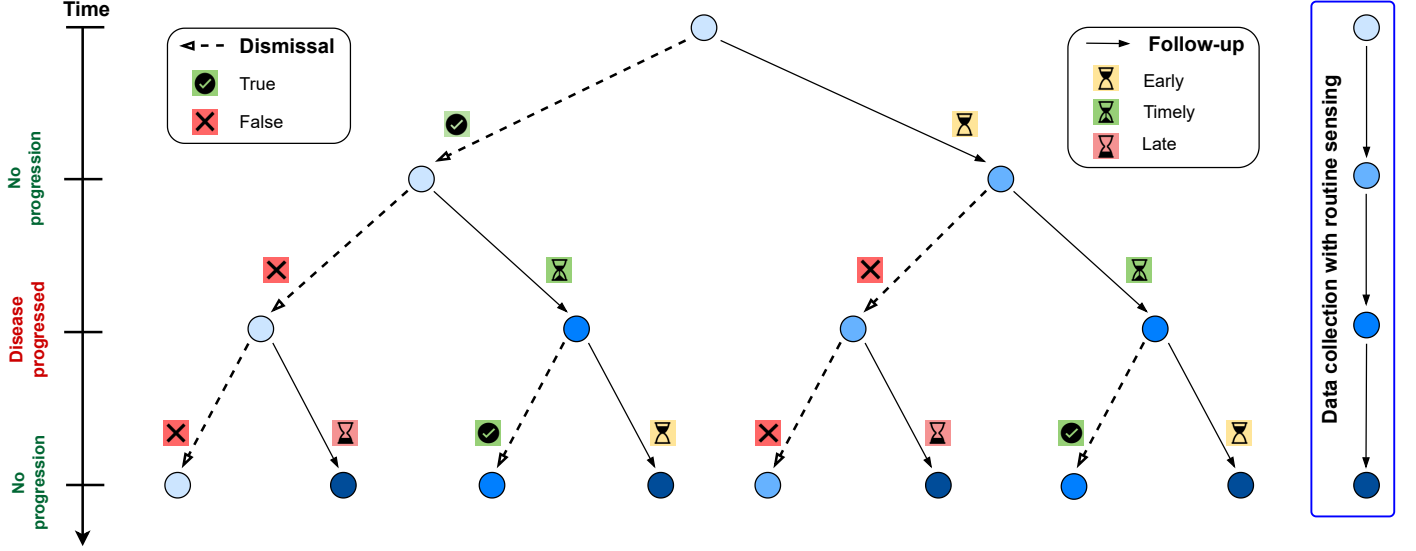


Fig. 2: Active sensing as decision-making, highlighting how present decisions to collect data impact future ones.

Q-learning. To measure the expected return of taking action a_t at state s_t according to policy π , we introduce a state-action value function:

$$Q_\pi(s_t, a_t) = r_t + \gamma Q_\pi(s_{t+1}, a_t). \quad (2)$$

When solving an MDP, we aim to obtain the optimal policy π^* . In the case of Q-learning (Watkins and Dayan, 1992), $\pi(s) = \delta_{\text{Dirac}}(\arg\max_a Q(s, a) = a_t^*) \forall s \in \mathbf{S}$, where $\delta_{\text{Dirac}}(\cdot)$ is the Dirac's delta function and a_t^* is the optimal action. For π^* , one can derive the Bellman equation as

$$Q^*(s_t, a_t) = r_t + \gamma \max_{a_{t+1}} Q^*(s_{t+1}, a_{t+1}). \quad (3)$$

Q-learning updates the Q-value for a certain action using the immediate reward and the maximum possible Q-value for the next state. Let us denote the post-update Q-value as $\tilde{Q}(s_t, a_t)$, the learning update is then:

$$\tilde{Q}_*(s_t, a_t) \leftarrow (1 - \alpha) Q_\pi(s_t, a_t) + \alpha \left(r_t + \gamma \max_a Q_\pi(s_{t+1}, a) \right), \quad (4)$$

where α is the learning rate, determining how much newly obtained information replaces the old information. Through interactions with the environment, the policy under Q-learning is supposed to converge after a sufficient number of iterations (Watkins and Dayan, 1992). The presented update rule is sufficient when the number of states and actions is relatively small. In the context of this study or other real-world

cases, the set of states may have an infinite size, making it impossible to store the Q-table.

Q-function approximation. In contemporary RL, the Q-function is often approximated by a neural network (NN) (Tesauro et al., 1995; Mnih et al., 2013, 2015), which we denote as $\tilde{Q}(s_t, a_t, \theta)$, where θ represents NN's parameters. The parameterized Q-function is then commonly called a Q-network. Mnih et al. (2013) introduced a method with two networks that allow to follow the Temporal Difference Learning idea (Tesauro et al., 1995): the local Q-Network, approximating $Q(s_t, \cdot)$, and the target Q-Network, approximating $Q(s_{t+1}, \cdot)$. The local Q-Network is optimized by utilizing the mean square error loss to measure the difference between the estimated Q-value and the true one, noted as:

$$\mathcal{L}(\theta) = \left\| r_t + \gamma \max_a Q(s_{t+1}, a, \theta^*) - Q(s_t, a_t, \theta) \right\|_2^2. \quad (5)$$

The parameters θ^* of the target Q-Network are updated periodically using the local Q-Network to stabilize the learning process and improve convergence.

Training Q-networks. To train a Q-network from various experiences and collect information along various roll-outs of an MDP, one has to balance exploration and exploitation during training. Here, we used an ϵ -greedy policy (Sutton and

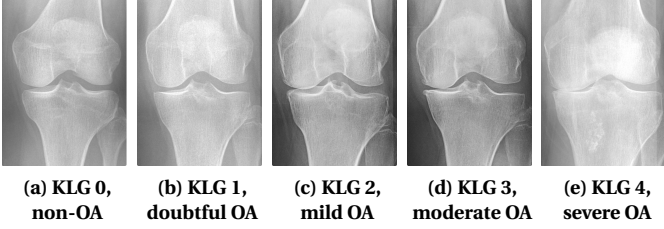


Fig. 3: Examples of knee radiographs depicting various stages of OA severity, categorized by KLG on a scale from 0 to 4. (a) KLG 0 – healthy knee joint, (b) KLG 1 – slight joint degeneration, (c) KLG 2 – noticeable joint space narrowing and definite osteophytes, (d) KLG 3 – severe joint space narrowing and presence of large osteophytes, (e) KLG 4 – the highest level of OA severity, where the joint space between the tibia and femur is minimal.

Barto, 2018) that induces the following action selection protocol. Let us draw $n_r \sim \text{Uniform}(0, 1)$, then

$$\pi(a_t | s_t) = \begin{cases} \arg \max_a Q(s_t, a) & \text{if } n_r < \varepsilon \\ \text{Random action} & \text{otherwise} \end{cases} \quad (6)$$

Here, $\varepsilon \in [0, 1]$ serves as a threshold for choosing an action, i.e. whether to follow the policy or take a risk and explore, based on a comparison with a randomly generated number in the range $[0, 1]$. Typically, ε is initialized at 1 and gradually decays over iterations until it reaches 0, indicating a transition from exploration to exploitation. The speed of this decay depends on the decay rate d_ε , such that $\varepsilon \leftarrow (1 - d_\varepsilon)\varepsilon$.

To improve the convergence of the training procedure, the experience replay technique is usually implemented (Watkins and Dayan, 1992; Mnih *et al.*, 2013, 2015). One typically stores experiences in a replay buffer so that the data that the agent collects in the past can be used for learning again and updating the network’s parameters.

2.3. Proposed method

Overview. To elaborate on our implementation of AS via Q-learning-based RL, we first define the state space and describe the reward function design. Subsequently, we provide details on the dataset used to construct the RL environment, the architecture of the model, and the considered hyper-parameters.

State space. We define the state $s_t \in \mathbf{S}$ as a combination of patient-level clinical variables, radiographic findings, and time indices of data acquisition (0 – baseline examination, 1

– 1-year follow-up, and so forth). The included clinical variables describe common risk factors: age, sex, and Body Mass Index (BMI). Furthermore, we used the Western Ontario and McMaster Universities Arthritis Index (WOMAC) to quantify the patient’s symptoms, the physical score of the 12-Item Short Form Survey (SF12) to quantify the overall patient’s physical condition, binary code about the occurrences of past knee injury and surgery. Previous studies have demonstrated that these factors are significantly associated with KOA progression (Eymard *et al.*, 2015; Joo *et al.*, 2022; Panfilov *et al.*, 2023).

The radiographs were automatically evaluated by a pre-trained DL model that extracts the Kellgren and Lawrence grading (KLG) system to derive KOA severity level (Kellgren and Lawrence, 1957). The KLG scale comprises 5 categories (from 0 to 4) that represent no OA, doubtful, mild, moderate, and severe OA, respectively. The graphical illustration of the KLG scale is provided in Figure 3. In our setup, we utilized the grades and their probabilities generated by a DL-based method developed for this task (Nguyen *et al.*, 2020).

Finally, beyond the clinical variables and image-related information (i.e. KLG), we included the time information as a part of the state, specifically, the current time index and the time index of the latest data acquisition. The clinical variables and the radiographic findings are updated in the state once the agent chooses a follow-up action.

Multi-progression. In this section, we introduce a procedure to construct a ground-truth set of progression events for individual subjects using the decline in medial fixed JSW@0.250¹, a robust and effective biomarker for capturing structural degeneration in KOA (Ratzlaff *et al.*, 2018). We use $\phi_L(\zeta)$ and $\phi_R(\zeta)$ to respectively denote the measured JSWs of the left and the right knees at every observational time point $\zeta \in \{0, \dots, T\}$. The changes in left and right JSWs at time point ζ relative to a reference time point ζ_r , where $\zeta_r < \zeta$, are denoted by $d_L(\zeta_r, \zeta)$ and $d_R(\zeta_r, \zeta)$, respectively. The following

¹Hereinafter, the two terms JSW and JSW@0.25 are used interchangeably.

procedure aims to generate the set of progression events \mathbf{M}_p , which was done once before training the RL policy.

Initially, we set the first reference time point to the baseline examination, denoted by $\zeta_r = 0$, and let \mathbf{M}_p be empty. At each time step $\zeta \in \{1, \dots, T\}$, we calculate $d_L(\zeta_r, \zeta)$ and $d_R(\zeta_r, \zeta)$ as follows:

$$d_L(\zeta_r, \zeta) = \max(0, \phi_L(\zeta_r) - \phi_L(\zeta)), \quad (7)$$

$$d_R(\zeta_r, \zeta) = \max(0, \phi_R(\zeta_r) - \phi_R(\zeta)). \quad (8)$$

Next, we define the patient-level KOA worsening at ζ relative to ζ_r as:

$$d_{LR}(\zeta_r, \zeta) = \max(d_L(\zeta_r, \zeta), d_R(\zeta_r, \zeta)). \quad (9)$$

If $d_{LR}(\zeta_r, \zeta)$ exceeds a threshold κ , a KOA progression event is recorded, and we add ζ to \mathbf{M}_p . We then set ζ as the new reference time point (i.e., $\zeta_r := \zeta$) and continue the procedure at $\zeta + 1$. If the threshold κ is not exceeded, the procedure also advances to $\zeta + 1$. Ultimately, when ζ reaches T , we terminate the process and obtain the progression set \mathbf{M}_p containing the time points of all the progression events.

Monetization of bilateral structural KOA progression. In this section, we aim to harmonize two semantically distinct units – bilateral structural changes (measured in mm) and acquisition costs (measured in \$) – in our reward function. Leveraging domain knowledge, we propose a novel approach to convert JSW reduction to a monetary value. Specifically, we assume that (1) the end-stage of the disease is TKR, and (2) if KOA is detected early, it can presumably be slowed down (Yao *et al.*, 2023). From these assumptions, we define c as the monetary loss of 1mm of articular cartilage (MLAC), calculated as:

$$c = \frac{\text{TKR cost (\$)}}{\text{Mean JSW of healthy knees (mm)}}, \quad (10)$$

where the mean JSW can be computed from an observational cohort and TKR cost is pre-defined for a healthcare system where the RL method is deployed. To this end, we can map bilateral structural changes (see eq. (9)) into financial costs as

$$\delta(\cdot, \cdot) = cd_{LR}(\cdot, \cdot). \quad (11)$$

Reward function. Given the set of progression events \mathbf{M}_p and the monetized radiographic changes, we here develop a novel reward function to optimize the AS objective stated in Section 2.1. This reward function is designed to provide our agent with *monetary* costs of its decisions by combining the costs from bilateral structural changes in the knees and acquisition costs.

For each subject, at time point $t \geq 0$, an agent takes one of two actions – to follow up or to dismiss (i.e. skip examination) at time $t + 1$. The rewards for these actions are denoted as r_f and r_d , respectively. The reference point t_r is updated to the latest visit, ensuring that the reward calculations are based on the most recent state of the subject's condition. By comparing $t + 1$ with t_p – the nearest progression time point t_p extracted from the patient-level progressions set \mathbf{M}_p , we derived five possible scenarios. Namely, there are three cases for the correctness of the follow-up action ($a = 1$): *early visit*, *timely visit*, and *late visit* and two cases for the one of the dismissal action ($a = 0$): *true dismissal* and *false dismissal*.

Mathematically, the reward r_t at the time point t corresponding to the follow-up and dismissal actions can be expressed as follows:

$$r_f = \begin{cases} e^{-\tau(t)} \Delta(t_r, t+1) - \lambda & \text{if } t+1 < t_p \text{ (early visit)} \\ \Delta(t_r, t+1) - \lambda & \text{if } t+1 = t_p \text{ (timely visit)} \\ -\alpha e^{\tau(t)} \Delta(t_r, t_p) - \lambda & \text{if } t+1 > t_p \text{ (late visit)} \end{cases} \quad (12)$$

$$r_d = \begin{cases} \beta & \text{if } t+1 < t_p \text{ (true dismissal)} \\ -e^{\tau(t)} \Delta(t_r, t_p) & \text{if } t+1 \geq t_p \text{ (false dismissal)}, \end{cases} \quad (13)$$

where $\Delta(t_r, \cdot)$ is the data acquisition utility function, representing the cost of significant changes relative to t_r , formulated as:

$$\Delta(t_r, \cdot) = \begin{cases} \delta(t_r, \cdot) & \text{if } \delta(t_r, \cdot) \geq c\kappa \\ 0 & \text{otherwise,} \end{cases} \quad (14)$$

$\lambda \in \mathbb{R}^+$ is the fixed cost of data acquisition. The reward for a late visit is equivalent to that for a false dismissal, yet discounted by $\alpha \in [0, 1)$ and decreased by λ . In addition, $\beta < c\kappa$ is the positive reward for the correct dismissal action.

To incorporate the difference between the time of making decision t and the true KOA progression time t_p into the reward function, we introduce the modulating function $\tau : [0, T] \rightarrow [0, 1]$, defined as:

$$\tau(t) = \frac{|t+1 - t_p|}{T}. \quad (15)$$

As such, we consider two specific cases that require such a modulating function: early follow-up and late follow-up/false dismissal. For the first case, we use an exponential decay function $e^{-\tau(t)}$. Therefore, an increasing $\tau(t)$ reduces the reward that an agent can obtain. For the second case, we penalize late or false dismissal actions and use the term $-e^{\tau(t)}$. As $\tau(t)$ increases, the negative reward becomes more considerable, discouraging the agent from delaying necessary actions or incorrectly dismissing the patient.

3. Related work

3.1. Knee osteoarthritis

In the KOA research area, there has been a growing interest in the application of machine learning (ML) methods for KOA progression prediction (Tiulpin *et al.*, 2019a; Tolpadi *et al.*, 2020; Guan *et al.*, 2020; Leung *et al.*, 2020; Jamshidi *et al.*, 2021; Tiulpin *et al.*, 2022; Nguyen *et al.*, 2022, 2023; Panfilov *et al.*, 2022, 2023; Cigdem and Deniz, 2023; Hirvasniemi *et al.*, 2023; Panfilov *et al.*, 2023). Two main lines of work related to the prediction of KOA progression from clinical and imaging data are the prediction of TKR (Tolpadi *et al.*, 2020; Leung *et al.*, 2020; Jamshidi *et al.*, 2021) and prediction of radiographic KOA worsening (Tiulpin *et al.*, 2019a; Guan *et al.*, 2020; Nguyen *et al.*, 2023).

TKR is an acknowledged clinical endpoint for KOA prediction, defining the ultimate stage of disease progression. However, the decision to operate is made based on symptomatic and functional assessment of the joint, as well as access to care. The time of TKR is therefore challenging to predict, due to the large amount of noise in the data. Tiulpin *et al.* (2019a) proposed to use KLG-based progression as an outcome, which was further studied by Nguyen *et al.* (2022, 2023) and Panfilov *et al.* (2022, 2023). The latter studies introduced

the CLIMAT method, showing that one can forecast the whole evolution of KLG scores using a transformer-based architecture.

The main limitation of most previous studies on KOA progression prediction is that they consider predictions per knee, disregarding that OA often co-occurs in two knees. The second limitation is that they ignore the long disease progression timelines, taking only the baseline measurement point for modeling. OA can progress very slowly, and be drastically accelerated by various future unknown factors, e.g. injury (?). Therefore, we believe that it is crucial to update the model's predictions when newer data from a patient becomes available. Finally, none of the previous studies considered the financial aspect of their results, nor downstream drug development or clinical applications. Our work aims to address all these limitations, enabling dynamic patient-level data collection, while balancing data collection utility and costs with RL.

The literature on AS falls into three main areas: recurrent neural networks (RNNs), Bayesian optimization, and RL. Additionally, we discuss KOA prognosis studies as prior knowledge for our work.

3.2. Active sensing

Recurrent neural networks. Considering AS as a sequential data collection prediction problem, RNN emerges as a natural approach. The inherent feedback loop in a standard RNN allows the model to memorize previous inputs, making it particularly effective with time-series data. Among the RNNs family, Gated Recurrent Unit (GRU) (Chung *et al.*, 2014) and Long Short-Term Memory (LSTM) (Hochreiter and Schmidhuber, 1997) are the most well-established methods and influential in various domains (Kollias *et al.*, 2018; Karita *et al.*, 2019). These methods have proven valuable, forecasting caring trajectories from medical records (Pham *et al.*, 2017). An LSTM-based model was developed to personalize clinical events prediction for ICU patients from electronic health records (Lee and Hauskrecht, 2023). Reddy and Delen (2018) proposed RNN-based methods to predict hospital readmission for lupus patients. Even though these studies created

benchmarks for an AS strategy, converting model predictions into decisions remains challenging due multi-objective nature of clinical decision-making (Sun and Giles, 2001).

Bayesian optimization. From the perspective of decision-making, Bayesian optimization (Ahmad and Yu, 2013; Alaa and Van Der Schaar, 2016; Pei et al., 2018; Jarrett and Van Der Schaar, 2020) is a powerful tool to tackle AS challenges. Ahmad and Yu (2013) introduced Context-Dependent Active Controller (C-DAC) – a Bayes-optimal decision-making model that aims to minimize behavioral costs, such as temporal delay, response error, and sensor repositioning cost for AS. Jarrett and Van Der Schaar (2020) introduced the concept of inverse AS, which seeks to uncover an agent’s preferences and strategy given their observable decision-making behavior. While these studies contribute foundational knowledge to AS in the medical area, they remain largely theoretical and lack performance validation on real clinical datasets with high-dimensional data.

Reinforcement learning. RL has become one of the most common techniques to explore AS in recent years, particularly in medical applications for disease management (Ahuja et al., 2017; Yoon et al., 2019; Chang et al., 2019; Qin et al., 2024; Holt et al., 2024). DPSCREEN framework proposed by Ahuja et al. (2017) aimed to deliver a personalized screening policy for breast cancer (BC) patients. The proposed policy utilizes both patient features and their clinical history, and it demonstrated significant reductions in the number of screenings performed while maintaining the same expected delays in disease detection. A similar problem of BC screening was also later tackled by (Yala et al., 2022).

Yoon et al. (2019) performed the AS using the Actor-Critic (ASAC) framework to tackle the issue of selecting the variables that should be observed. The ASAC framework includes two networks: a selector network, playing as an actor, and a predictor network, playing as a critic. The authors showed that ASAC outperformed state-of-the-art methods in two real-world medical datasets of Alzheimer’s Disease and electronic health records.

Chang et al. (2019) presented a deep Q-learning approach to strategically schedule measurements, especially in ICU mortality prediction. In simulations and real-world datasets, the proposed policy outperforms heuristic-based scheduling with higher predictive gain and lower cost.

The prior work on AS with RL focused on improving general RL methods and placed a substantially lesser focus on the reward function, the disease of interest, as well as the challenge of handling high-dimensional data. In this work, we chose a simple and the most common RL technique – Q-learning and focused on the development of the reward and the environment for the target domain of KOA.

4. Experimental setup

4.1. Dataset

We conducted experiments on the Osteoarthritis Initiative (OAI) dataset, publicly available at <https://nda.nih.gov/oai/>. Since the OAI is a multi-center cohort, we chose one center as our test set, and the remaining data served for training purposes. To conduct our AS experiments, we included data from the baseline, 1-year, 2-year, 3-year, and 4-year follow-ups.

Each included participant had bilateral plain radiographs, and we used the method developed by Tiulpin et al. (2019b) to localize the knee joints (Nguyen et al., 2022, 2023; Tiulpin et al., 2019a). We included only those subjects whose knee images and all the listed clinical data were fully available. To track the disease progression, we employed JSW, easily collected from radiographs and available in OAI. The KLG scores, representing the severity of KOA disease, were computed from a DL-based model (Nguyen et al., 2020). Furthermore, we utilized clinical data including age, sex, BMI, physical SF12 score (Ware et al., 1996), past injury records, past surgery records. To aid the models with the status of the joint function, stiffness, and pain, we also employed the total WOMAC score (Bellamy et al., 1988) in our feature vector. After the data curation, we obtained the radiographs and the clinical variables from a total of 1620 OAI participants. The data statistics at the baseline are summarized in Table 1.

Table 1: Characteristics of the OAI participants’ data at the baseline. (★) Participants were classified as “Asymptomatic” if they obtained a WOMAC score of 0, and “Symptomatic” otherwise. (★★) Participants’ KOA severity was classified based on the KLG system at the baseline. Those with both knees obtained KLG 0/1 are labeled as “Healthy”, while individuals with at least one knee graded KLG 2, KLG 3, or KLG 4 are categorized as “Mild”, “Moderate”, or “Severe” KOA, respectively.

Category	Sub-groups	Training	Test
Subjects	-	1199	421
Knees	-	2398	842
Age	< 55	345 (28.8%)	103 (27.6%)
	54-64	404 (33.7%)	134 (31.8%)
	65-74	359 (29.9%)	146 (34.7%)
	> 75	91 (7.6%)	38 (9.0%)
Sex	Male	488 (40.7%)	180 (42.8%)
	Female	711 (59.3%)	241 (57.2%)
BMI	Underweight	2 (0.17%)	1 (0.24%)
	Healthy	248 (20.7%)	98 (23.28%)
	Overweight	471 (39.3%)	185 (43.9%)
	Obesity	478 (39.7%)	137 (32.5%)
Symptomatic(★)	Yes	1006 (83.9%)	340 (80.8%)
	No	193 (16.1%)	81 (19.2%)
Severity(★★)	Healthy	344 (38.7%)	120 (28.5%)
	Mild	452 (37.7%)	171 (40.6%)
	Moderate	345 (28.8%)	109 (25.9%)
	Severe	58 (4.8%)	21 (5.0%)

4.2. Hyper-parameters of the reward function

We utilized the Current Procedural Terminology (CPT) system in the United States to search for the expenses associated with medical imaging and TKR (Thorwarth Jr, 2004; Hirsch et al., 2015). Based on these data, the TKR surgery (CPT code: 27446) can amount to up to \$50,000 per patient. A follow-up visit consisting of consultant fees (CPT code: 73560) and a knee X-ray imaging (CPT codes: 73560, 73562, 73564, 73565) may range from \$300 to \$1,000. The medical cost varies depending on region, insurance, and other caring services. In our experiments, we empirically set the cost of TKR at \$10,000, and the cost of each hospital visit at \$500.

The average healthy JSW was set to 5mm according to Buckland-Wright et al. (1995); Anas et al. (2013). We compute the parameter c in Eq. (10) as $c = \$10,000/5\text{mm} = 2000\$/\text{mm}$. For numerical stability, we scaled down all monetary hyper-parameters by 1000.

We empirically chose $\alpha = 0.5$ as a parameter to scale down the late visit-associated negative reward and set $\beta = 0.3c$ to assign positive rewards for correct dismissal. $\lambda = 0.5$ was used

Table 2: The statistics of subjects progressed with KOA in the training and test sets after the baseline examination

Year(s)	1	2	3	4
Training set	161 (13.4%)	211 (17.6%)	242 (20.2%)	233 (19.4%)
Test set	49 (11.6%)	53 (13.6%)	52 (12.4%)	64 (15.2%)

in all our experiments, and we also conducted an ablation study to validate how our method performs in different settings. More details about these hyper-parameters will be presented in Section 5.2.

4.3. Agent

We designed our Q-Network to process the state revealed by the environment (i.e. multi-modal input data) and predict the Q-value for each action. The input data, excluding the KOA status, were normalized across the dataset by subtracting the mean and dividing by the standard deviation. The KOA status, as presented in Section 2.3, is a vector of probabilities extracted from a pre-trained deep neural network (DNN), where each probability corresponds to a particular severity grade. We employed the Semixup model (Nguyen et al., 2020) to extract image features and KLG probabilities. Whereas the imaging feature dimension of each radiograph was 1024, the vector of KLG probabilities had a size of 5.

We first combined the KLG probability vectors from both knees and the vector of clinical variables, resulting in an input vector of size 22. The Q-Network was a simple neural network a simple neural network (batch norm of the inputs followed by a single hidden layer with dropout probability of 0.2 and sigmoid activation function, followed by a linear output layer with 2 heads). The network’s output was a 2-element vector representing Q-values of 2 actions for each time step.

The agent was trained in an episodic setting, where each episode represented a subject’s participation in an observational study. We performed the training over 1000 epochs, each of which is a complete traverse through the whole training set. To prevent the agent from memorizing the order of the data, we shuffled them at the start of each epoch. During every episode, the agent interacted with the environment a finite number of times T , thereby generating experiences

Table 3: Comparison between our RL policy and the baseline approaches by individual gain (reward - RPP), acquisition costs, and average balanced accuracy (BA), average recall (RC) in designing personalized AS schedules for KOA patients. We categorized 3 types of policies: random, routine, and active policies. (*) indicates a binomial distribution with $n = 4$. The highest score for each metric is underlined. Bold figures indicate the top scores among AS policies.

Type of sensing	Method	RPP \uparrow	Acquisition cost \downarrow	Average BA \uparrow	Average RC \uparrow
Random*	$p(a = 1) = 0.3$	-0.78 ± 0.06	0.59 ± 0.01	50.42 ± 0.49	30.15 ± 0.87
	$p(a = 1) = 0.5$	-0.65 ± 0.05	1.00 ± 0.01	49.69 ± 0.46	49.48 ± 0.88
	$p(a = 1) = 0.7$	-0.56 ± 0.04	1.40 ± 0.01	50.73 ± 0.51	71.15 ± 0.96
	$p(a = 1) = 0.9$	-0.72 ± 0.01	1.79 ± 0.00	50.28 ± 0.34	90.09 ± 0.60
Routine	NS	-1.64	<u>0</u>	50	0
	BAS	-0.10	1	50	50
	ANS	-0.86	2	50	<u>100</u>
Active	LR	-0.85	0.74	50.02	37.07
	Cox	-0.86	0.40	53.80	19.27
	DeepHit	-0.29	1.18	52.39	62.98
	GRU	-1.23 ± 0.10	0.24 ± 0.07	52.79 ± 0.45	17.00 ± 4.22
	LSTM	-1.34 ± 0.08	0.12 ± 0.02	52.30 ± 0.74	9.74 ± 2.43
	CLIMATv2	-0.54 ± 0.04	0.53 ± 0.04	56.41 ± 0.41	37.78 ± 2.27
	RL (Ours)	<u>0.20 ± 0.03</u>	1.11 ± 0.02	<u>60.33 ± 0.32</u>	<u>73.67 ± 1.00</u>

comprising states, actions, and rewards. These experiences were stored in a replay buffer with a capacity of 10^4 . For every 50 episodes, we randomly sampled a batch of 256 experiences from the replay buffer to train the network. We employed the mean square error loss and the Adam optimizer (Kingma and Ba, 2014) with an initial learning rate of 5×10^{-4} .

4.4. Evaluation

We compared our method to a wide range of reference methods belonging to three categories of sensing – random, routine, and active sensing. Random policies combined 4 probabilities of taking follow-up action: 0.3, 0.5, 0.7, and 0.9. The set of routine policies comprised “no sensing” (NS), annual sensing (ANS), and bi-annual sensing (BAS). The active policies set included logistic regression (LR), cox regression (CR), RNN-based methods, and CLIMATv2 (Nguyen et al., 2022, 2023). The reference methods are described in detail in Section S1.1.

We validated the policies using the Reward Per Person over 4 years (RPP), formulated as follows

$$\bar{R} = \frac{1}{N} \sum_{i=1}^N \sum_{t=0}^T r_t^{(i)}, \quad (16)$$

where N is the number of subjects. RPP represents the monetary utility that each subject with KOA can earn or overspend

on AS. To quantitatively evaluate the correctness of the policies, we calculated the balanced accuracy (BA) and recall (RC) scores at each time step and averaged them across all the follow-ups. We repeated our experiments using 10 different random seeds and reported the average results along with their standard errors across the runs.

5. Results

5.1. Comparisons to reference methods

We present the quantitative comparisons between our method and the baselines in Table 3. The random policies generally could not exceed 51% of the average BA, regardless of 4 different probabilities of selecting the follow-up action. As the probabilities increased from 30% to 90%, the trend of RPP exhibited a parabolic shape, peaking at 70%. The RPP of 30% and 90% probabilities were approximately equal to each other, and these were the lowest among the random policies under consideration. This suggests a non-linear relationship between the selection probability and the policy performance.

Among the three routine sensing approaches, the BAS policy yielded the highest reward, yet it was still a negative reward of -0.1 . The NS policy resulted in the lowest reward not

only among the three but also across all the methods. When replacing the BAS with the random policy, we observed an increase of 2.97% in BA, albeit drops of 3.34% in RC, and 0.66 in reward. The ANS policy, which ensured no missed follow-up visits, led to the highest acquisition cost compared to all the methods. Compared to this policy, our method was able to identify 73.67% of the progressions while reducing the acquisition cost by up to 45.5%.

In general, AS baselines tended to enhance BA yet deteriorate RC when compared to the BAS policy. Specifically, the improvement in BA ranged from 0.02% to 6.41%, with the most significant increase observed in CLIMATv2. However, DeepHit was the only AS reference that improved RC compared to the BAS policy, demonstrating an increase of 12.98%. As a result, DeepHit achieved the highest reward among all the baselines, although its total reward was still negative.

Different from the AS baselines, our RL-based policy led to improvements in both BA and RC. Specifically, our method significantly outperformed CLIMATv2 with increases of 3.9% in BA and 35.9% in RC. When compared to DeepHit, the RL-based method demonstrated substantial improvements of 7.9% in BA and 10.7% in RC. Notably, our method was the only one that gained a positive reward, with a value of 0.2.

5.2. Impact of financial factors on decision-making

As the cost-related parameters, λ and c , are key factors in our reward function, we aimed to quantitatively assess their impacts on our method. Specifically, we conducted two experiments involving our proposed methods, CLIMATv2, ANS, and NS policies. In the first experiment, we varied the hospital visit cost, λ , while keeping the MLAC, c , unchanged. In the second experiment, we reversed the settings.

We present the results of the first experiment in [Figure 4a](#), demonstrating the association between λ and the RPP over 4 year, with a fixed c of 2. Generally, all methods exhibited a decreasing trend in the reward as the hospital visit cost increased. Compared to the mentioned baselines, our RL-based method, corresponding to the blue curve in [Figure 4a](#), consistently gained better rewards per person with

every value of $\lambda \in [0, 2]$. The NS policy, displayed in black, resulted in a constant reward of -1.64 per person since no follow-up data was acquired. Increasing λ from 0 to 1.5 caused a significant drop of approximately 6.0 in the RPP of the ANS policy. Our proposed method met the ANS policy at $\lambda = 0$ and approached the NS policy when λ increased.

We demonstrate the results of the second experiment in [Figure 4b](#). The performance of CLIMATv2 and the NS policy exhibited a decreasing trend as the JSW cost, c , increased while keeping unchanged $\lambda = 0.5$. In contrast, we observed that the ANS policy generally increased in proportion to c . Our policy achieved a constant reward of -0.25 for $c \leq 1.0$, and demonstrated a linear increase for $c > 1.0$. Overall, our proposed policy gained the highest reward among the methods at any value of $c \in [0.5, 2]$. For values of c greater than 1.5, our method stands out as the sole approach yielding positive rewards per person.

To gain deeper insights into the trade-offs related to the cost parameters λ and c , and their impact on the outcomes, we investigated the relationship between the relative cost $\frac{\lambda}{c}$ and the resulting RPP normalized over the hospital cost, $\frac{\bar{R}}{c}$. Specifically, we varied the hospital visit cost parameter, λ , across the range $\{0, 0.25, 0.5, 0.75, 1, 1.5, 2, 2.5, 3, 3.5, 4\}$, while adjusting the MLAC, c , within the set $\{0.5, 1, 1.5, 2, 3, 4\}$. The association is illustrated in [Figure 4c](#). We observed that $\frac{\bar{R}}{c}$ exhibited an inverse, non-linear relationship with the increasing of $\frac{\lambda}{c}$. In other words, decreasing $\frac{\lambda}{c}$ was beneficial for the resulting RPP. Specifically, when the ratio $\frac{\lambda}{c}$ declines to 0.3, it becomes the critical trade-off point at which our policy begins to yield positive RPPs. The raw experimental data behind [Figure 4c](#) is shown in [Suppl. Section S1.2](#)

5.3. Patient-level versus knee-level predictions

Most previous studies on KOA prognosis assessed the development of KOA within a single knee. However, we argue that for improved health outcomes it is essential to incorporate information from both knees into patient-level inputs. Therefore, we conducted an experimental comparison of the knee-level against and the patient-level approach us-

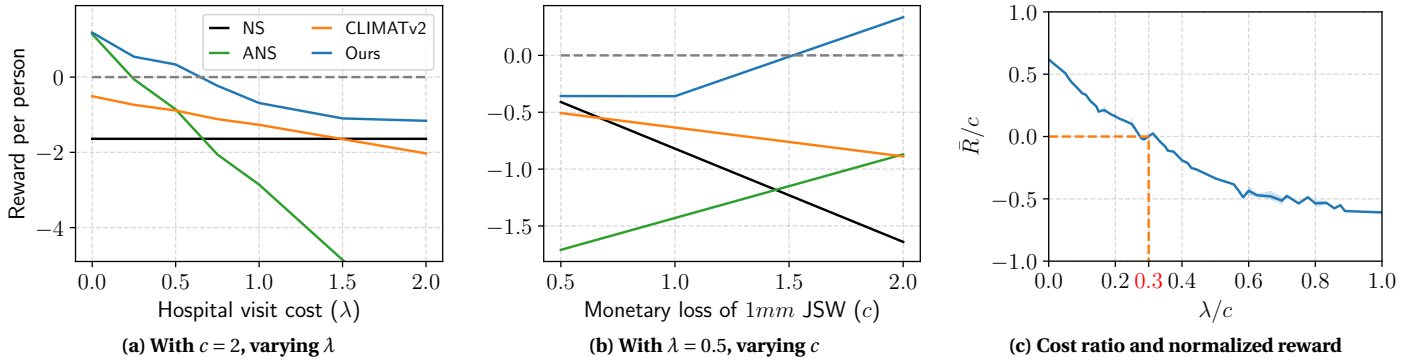


Fig. 4: The reward per person of “no sensing”, annual sensing, CLIMATv2, and our policy by adjusting (a) the hospital visit cost from \$0 to \$2,000; (b) the cost of 1mm JSW degeneration from \$500 to \$2,000 which correlated with the increase of TKR cost; (c) the relationship between the cost ratio (λ/c) and the JSW reward (\bar{r}/c) achieved by our RL-based method. The parameters have been varied in both training and testing (deployment) datasets. We found that the ratio λ/c of 0.3 is a threshold for a cost-efficiency policy (highlighted in red).

Table 4: Overall performances of our RL-based methods and CLIMATv2 on knee-level and patient-level approaches.

Approach	Method	Reward	BA	Recall
Knee-level	CLIMATv2	-0.56	54.97	33.20
	Ours	0.18	56.60	53.32
Patient-level	CLIMATv2	-0.54	56.41	37.78
	Ours	0.20	60.33	73.67

ing our proposed method and a state-of-the-art baseline CLIMATv2 (Nguyen *et al.*, 2023).

As we aimed to perform the patient-level progression prediction to assist a personalized follow-up plan, we still evaluated all policies at the knee-level. In the knee-level approach, we implemented 2 individual agents to predict the degeneration of each knee side. The final decision in the evaluation step was made by combining the actions of two knee-side agents, following the rule that any progression in either knee triggers a progression event.

Table 4 demonstrates the overall performance of CLIMATv2 and our proposed method with knee-level and patient-level approaches (see Suppl. Table S1 for raw data). Notably, the patient-level approach outperformed the knee-level approach for both CLIMATv2 and the RL-based policy, with average improvements in BA of 1.44% and 3.73%, respectively, and in RC of 4.58% and 20.25%, respectively. Both the methods gained a 0.02 increase in RPP when switching from the knee-level to the patient-level approach.

To provide additional insights, we further present the cor-

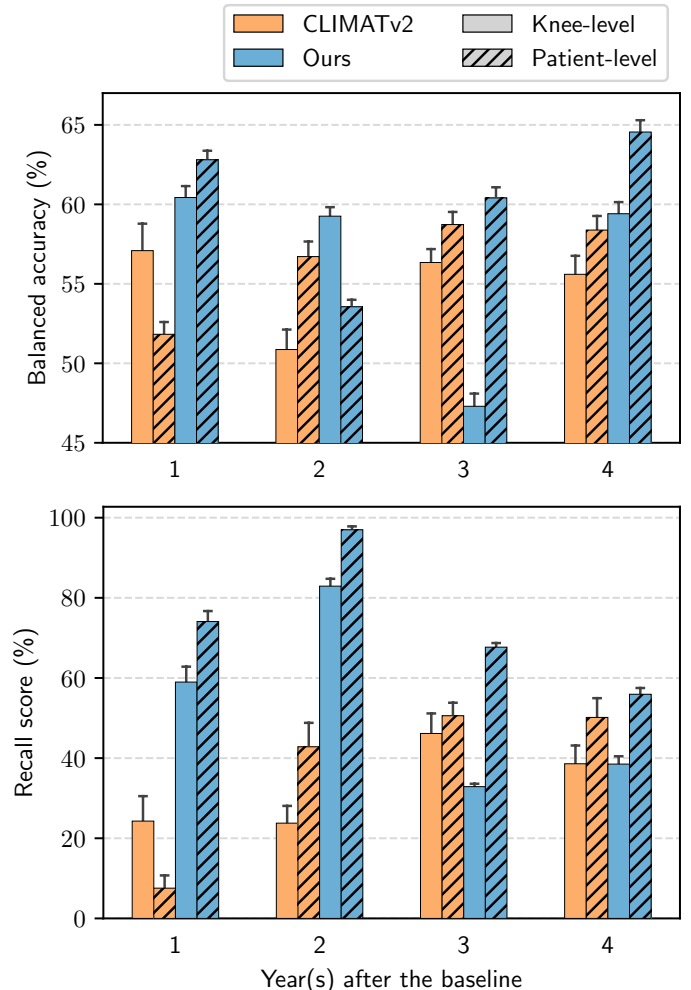


Fig. 5: Accuracy metrics of knee-level approach and patient-level approach at each follow-up year after the baseline visit. The error bars represented the standard error of 10 random seed runs.

responding fine-grained results in Figure 5. Most of the time, patient-level models reduced the standard error in BA and RC of both CLIMATv2 and our RL-based agent. Particu-

Table 5: Performance of our RL-based method on the deployment set with various types of radiographic findings. The benchmark is a setting without images. The remaining experiments involved manual KLG and automatic KLG, serving as KOA findings. Automatic KLGs were extracted from a pre-trained DNN under image features or probabilities.

Input	Reward	Average BA	Average Recall
Without imaging	-0.05 ± 0.03	55.02 ± 0.30	66.87 ± 1.53
KLG Ground truth	0.15 ± 0.02	57.69 ± 0.27	64.53 ± 1.33
Image features	-0.86 ± 0.03	51.91 ± 0.41	26.62 ± 1.16
KLG probabilities	0.20 ± 0.03	60.33 ± 0.32	73.67 ± 1.00

larly, at the 1-year time point, our patient-level policy exceeded the patient-level CLIMATv2 with the highest difference by approximately 15% in BA and 60% in RC. Furthermore, the greatest gap between patient-level and knee-level of our method occurred 3 years after baseline by approximately 20% in BA and 40% in RC. In general, our patient-level policy showed substantial improvement compared to other methods most of the time.

5.4. Importance of imaging data

We also evaluated the impact of imaging data on the performance of the proposed method. To set up a benchmark, we conducted experiments without the contributions of radiographs, thereby excluding the KLG probabilities from the agent’s input. We then incorporated one of the three distinct types of KLGs into our experiments. The first type, referred to as the “KLG ground truth” corresponds to the manual grades produced by the radiologists. The second and third types named the “image features” and the “KLG probabilities”, respectively, were extracted from a DNN that had been trained to predict the KLGs from radiographs automatically (Nguyen *et al.*, 2020).

Table 5 illustrates the performance of our RL-based method when the image-derived data type changes. Specifically, the setup in which the imaging data were eliminated from the state completely, resulted in poor performance with a negative reward of -0.05 and an average BA of 55.02%. Meanwhile, using ground-truth KLG in states led to substantial improvements of 0.20 average reward and 2.67% average BA. When we used image features extracted from the network instead of the KLGs, we obtained a negative reward of -0.86

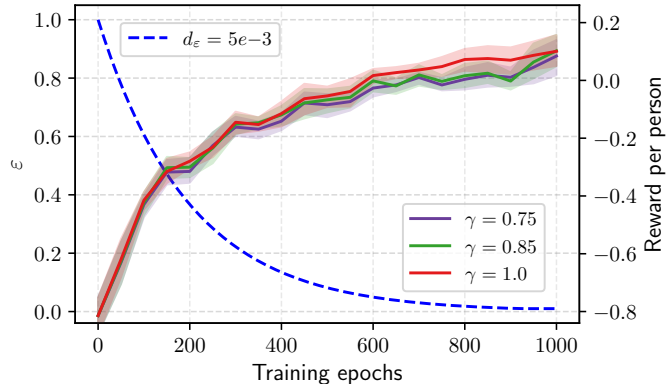


Fig. 6: Model training convergence. We adjusted exploration and exploitation by decaying ϵ over epochs with different discount factors γ . The dashed line indicates the decaying of ϵ corresponding to the left axis. The color lines, corresponding to the right axis, describe the improvement of RPP over 4 years under RL-based policy. Each color demonstrated the performance of each discount factor $\gamma \in \{0.75, 0.85, 1.0\}$. The policy trained by $\gamma = 1.0$ was the most stable one and achieved the highest reward over training.

and performance drops with an average BA of 51.91% and an average RC score of 26.62%. In contrast, having KLG probabilities in the state yielded a positive total reward of 0.20, and outperformed other setups with the average RC of 73.67%.

5.5. Training process convergence in an episodic setup

For the ϵ -greedy policy, we conducted the experiment where d_ϵ was selected from the set $\{1e-2, 5e-3, 1e-3\}$. Each setting was repeated with 10 random seeds. With 3 different ϵ decayed curves, the training policies converged yet at different training times. The convergence of training in any exploration-exploitation strategy serves as preliminary evidence of the effectiveness of our proposed reward function in identifying an optimal policy. By comparing the learning curve of 3 decaying ϵ greedy policies during 1000 epochs training, we concluded by choosing $d_\epsilon = 5e-3$, illustrated in Figure 6, as the most appropriate value to define the exploration-exploitation process within an acceptable training time.

Besides, an ablation study about the impact of the discount factor on learning progress was expressed in Figure 6 with similar exploration decaying. Our results showed that the values of $\gamma < 1.0$ for discounting future rewards was inefficient and even harmed the performance. $\gamma = 1$ was chosen for all the following experiments.

5.6. Reward function ablation

We performed an ablation study on the parameters α and β in our reward function. These parameters correspond to the *late visit* and *true dismissal* actions, respectively. Our experiment involved an evaluation on a grid, where $\alpha \in \{0.25, 0.50, 0.75, 1.00\}$ and $\beta \in \{0.1c, 0.3c, 0.5c, 0.7c\}$.

Given that the reward scale fluctuates with adjustments to these parameters, as indicated in Equations (12) and (13), we introduced the normalized score – recall-over-cost ratio as a metric for assessment of the results. For a comprehensive evaluation of accuracy, we utilized the BA score. The results are illustrated in Figure 7. Our findings revealed that the optimal parameter combination was $\alpha = 0.5$ and $\beta = 0.3c$. This combination yielded a BA score of 60% and a recall-over-cost ratio of 67%, the highest scores among other combinations.

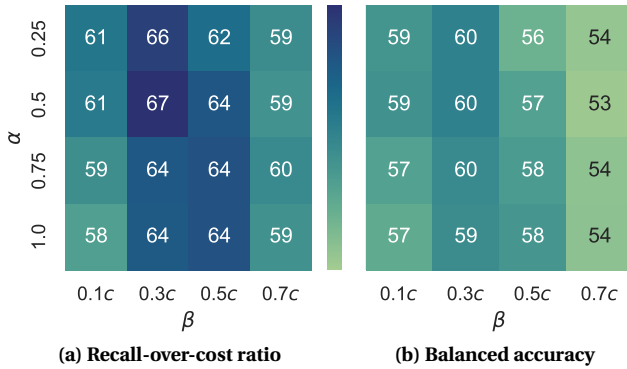


Fig. 7: Ablation studies on α and β , evaluating by the balanced accuracy and the ratio of RC over acquisition cost. We chose values of α and β based on these metrics.

5.7. Follow-up frequency

In this section, we assessed the dependency between the number of follow-up decisions made by our method and the disease characteristics. Specifically, Figure 8 visualizes the number of hospital visits per person according to individual KLG pairs measured at the baseline visit (see Suppl. Table S3 for raw data). Those KLG pairs are classified into 4 subgroups, denoted by color regions: "Healthy" when neither knee has KLG greater than 1, "Mild" when neither knee has KLG greater than 2, "Moderate" when neither knee has KLG greater than 3, and "Severe" when at least one knee has KLG 4. We illustrated

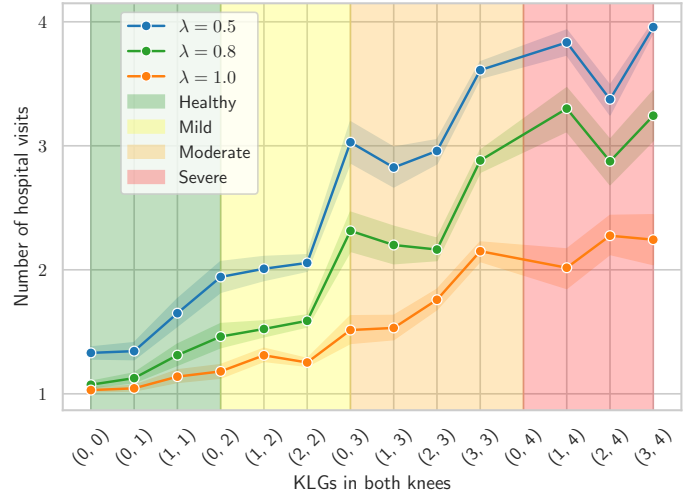


Fig. 8: Dependency between the baseline OA severity and the number of follow-up decisions. The horizontal axis arranges the increasing OA severity, with numbers in parentheses indicating the KLG for both knees, without specifying the side. Three lines in the graph represent 3 RL-based policies obtained at different hospital visit costs $\lambda = \{0.5, 0.8, 1.0\}$. The color-coded regions denote the patient-level of OA severity, where "Healthy" indicates neither knee has a KLG greater than 1, "Mild" indicates neither knee has a KLG greater than 2, "Moderate" indicates neither knees graded KLG greater than 3, and "Severe" indicates at least one knee has a KLG 4.

our policies with 3 different λ of 0.5, 0.8, and 1.0 by three lines in the graphs. All these policies delivered at least one follow-up to participants regardless of the costs. The diagram shows that our policy learned to be severity-aware, and realized that patients with more severe forms of OA in both knees progress faster. That is, the agent recommended more visits in such a case, and consistently in all considered cost settings.

Finally, we also analyzed the frequency of follow-up decisions over 4 years in various subgroups split based on sex, age, BMI, symptomatic status, and the ground-truth number of progressions. The results were drawn from the experiment mentioned in Section 4.2 and displayed in Figure 9. Specifically, every participant, irrespective of their subcategory, had at least one follow-up, which is consistent with Figure 9. However, we observed that males were more likely to have additional visits compared to females. In terms of BMI, participants classified as overweight or obese obtained a higher number of follow-ups compared to those with a healthy BMI. When considering symptomatic status, our policy selected more follow-up decisions for symptomatic patients than asymptomatic ones, indicating its responsiveness to symptom presence. Age-wise, the number of rec-

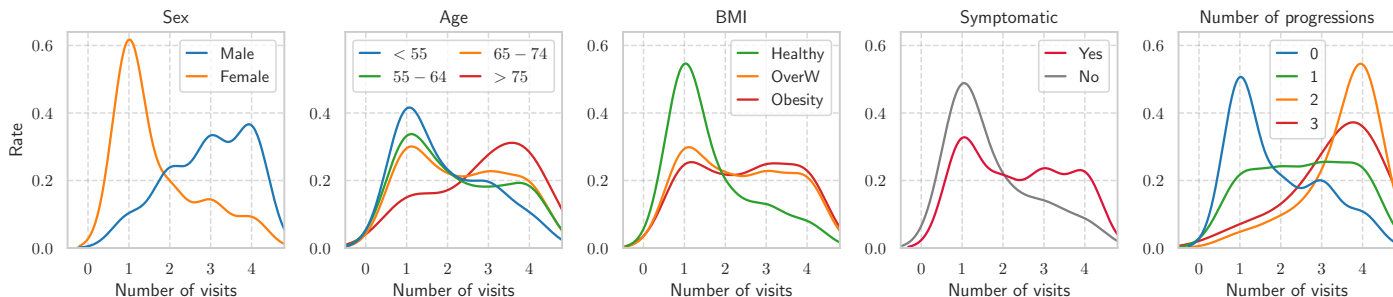


Fig. 9: The distribution of follow-up decision frequency (x-axis) in various categories with the visit cost of $\lambda = 0.5$. Particularly, “Age”, “BMI”, and “Symptomatic” were classified at the baseline. Our policy mostly recommended at least one follow-up in the course of 4 years for participants. A higher number of follow-up decisions were made for males compared to females, for overweight/obese individuals compared to healthy ones, and for those with symptoms compared to those without symptoms diagnosed at the baseline. Our proposed AS delivered several follow-up actions for participants who developed/progressed OA multiple times.

ommended follow-ups increased towards older participant groups, being the largest for the ones over 75 years old. When we compared the frequency of visits to the actual number of progressions, we found that participants with multi-progression were most likely to have frequent visits (4 times).

6. Discussion and conclusions

In this study, we developed an RL-based AS strategy, which allows for following up KOA patients for radiographic changes with high sensitivity and cost-efficiency. The core of our methodology is an episodic Q-learning approach with a novel reward function specifically designed for detecting patient-level disease progression with recurrent events in an online AS setting. Through extensive experiments, we showed that our method outperforms various baselines in terms of balancing disease outcomes and costs, and it is the only method to achieve a positive RPP. To the best of our knowledge, this work is the first to consider dynamic KOA progression monitoring, and it is the first work in the field of OA to tackle the issue of optimal data collection.

KOA is so far a non-reversible joint disease. The common trait of KOA progression is the narrowing of JSW, which is observable via various modalities. To detect and track KOA progression longitudinally, imaging techniques like X-rays, MRI, and CT scans are often employed (Roemer *et al.*, 2022). We proposed to connect quantitatively measured radiographic changes with data acquisition cost, aiming to define the utility of detecting a KOA progression event. Although quality-of-

life (QoL) measures can be more informative disease markers to track, the cause of pain at different stages of KOA is different (Roemer *et al.*, 2014), the relationship between pain, joint function, and imaging can change, thereby affecting the predictive model. Moreover, it is challenging to measure QoL objectively due to chronic pain having a psychosocially driven nature (Tanguay-Sabourin *et al.*, 2023). Hence, in our study, we concluded that the best available method to track the disease in OA is based on radiographs due to their wide accessibility, and ease of use.

Several radiographic imaging biomarkers, including the OARSI grade (Altman and Gold, 2007), the KLG system (Kellgren and Lawrence, 1957), and the JSW degeneration (Duryea *et al.*, 2010), are used to define OA progression, particularly, in KOA. These biomarkers track the disease progression within a single knee joint, however, we argue that a sensing policy should consider the evolution of OA in both knee sides simultaneously. Even though OA can develop in multiple joints, only a few studies so far focused on predicting progression at a patient level. Our study showed that an AS policy that tracks patient-level progression substantially outperforms knee-level one (Section 5.3). Moreover, we choose medial JSW@0.250 (Duryea *et al.*, 2010) as the disease biomarker, due to it being continuous and standardized, allowing us to establish more fine-grained associations between the changes in knee radiographs and monetary value.

In this work, we developed a reward function, which balances the ability of the agent to detect KOA progression and

the acquisition costs. The proposed reward incorporates follow-up and dismissal actions, divided into mutually exclusive scenarios that occur during the follow-up of the disease progression in a patient. However, we faced challenges in defining the value of true dismissal and late follow-up decisions as the disease statuses from those cases are unknown. To address the challenges, we introduced hyper-parameters α and β into our reward function. α mitigates the punishment for late follow-up over false dismissal (late better than none) and β represents the gained reward of true dismissal. We believe that α and β should be tailored to better fit different socio-economic contexts and applications, investigating which is beyond the scope of the present work.

Given the complexity of KOA progression, it is worth discussing the various sensing policies we implemented as baselines. The annual sensing, while thorough, may not be cost-effective as it incurs the highest acquisition costs. The BAS policy seems to be an ideal easy-to-implement policy cost-wise, but it detects only 50% of progressors. Implementing predictive models as a base for AS was expected to bring positive outcomes, however, the results did not yield a positive reward in any of the cases. In a general cost setting over 4 years, to collect over 70% of all progression events, the acquisition budget requires \$1,400 – \$2,000 for each participant, whereas our policy costs only around \$1,110, which would help to save approximately 21% – 45% of costs per patient in a trial. The flexibility in various financial factors is an outstanding advantage of our method compared to any method we compared it to. The quality of decision-making of our policy depends on the ratio of acquisition cost over treatment cost (λ/c). We found that all settings where $\lambda/c \leq 0.3$ are the ones giving positive rewards. This threshold may assist the clinical trial or experiment organizer in budgetary planning, directly connecting decision-making and costs.

We showed awareness of our policy regarding KOA characteristics such as disease severity, participant weight, and knee symptoms through more frequent follow-ups for patients at higher risk of OA. Interestingly, females are generally consid-

ered to be at higher risk of developing KOA than males (Pan et al., 2016; Contartese et al., 2020), albeit our policy selected more follow-ups for males. This observation can be partially explained by data bias in our test set. 30% of females were healthy in terms of BMI, while the ratio of males with healthy BMI was only 15%. A similar observation was done for KLG subgroups, where 32% of females but only 24% of males were diagnosed as healthy at the baseline visit. Therefore, as a risk factor, our policy prioritized BMI over sex in the decision-making. Interestingly, our policy tried to equalize the follow-up chance for everyone by recommending at least one follow-up even in the high visit cost scenario. Equalizing decisions can be considered as a drawback from the viewpoint of the data collection organizer.

Our study’s core novelty is in proposing RL-based AS for KOA progression monitoring. While we acknowledge certain areas for improvement, they also represent exciting opportunities for future research and development. Firstly, our method requires data from a longitudinal cohort for training. The scarcity of such data limits our ability to test with different populations. On the other hand, we were able to utilize openly available OAI cohorts, and thus think that the developed policies can be fine-tuned on specific data. Secondly, our policy adaptively changes in various cost settings, and it might not always yield positive outcomes, especially in cases when data acquisition cost is high. The presence of a “trade-off” point can be viewed as an upper bound of the monetary efficiency of an AS policy for KOA. Optimizing this bound will not only improve our model but will naturally result in new knowledge in the field of KOA. Thirdly, we recognize the potential of tracking also symptomatic biomarkers when assessing disease trajectory. As KOA often causes chronic pain, integrating imaging biomarkers with symptomatic ones might lead to more precise progression outcomes and, thus, more accurate progression modeling. Fourthly, our workflow used a pre-trained DNN model to predict KLG and extract probability for state input. While the performance of the pre-trained model can impact our results, it also high-

lights the importance of continual model refinement and improvement. However, for an RL workflow, working with high-dimensional data, such as plain radiographs, as the input state poses computational challenges. While we acknowledge the mentioned limitations, we view these not as obstacles but as motivations for innovation and improvement in our method.

To summarize, we have proposed a novel way to collect data for osteoarthritis trials utilizing RL. Our method requires no human input and can run fully automatically. We demonstrated that the proposed method outperforms existing baselines, and we evaluated different design choices through a set of comprehensive ablation studies. The developed approach to acquiring the next-generation data in OA shows promise in delivering more cost-effective clinical trials and observational studies in OA. Furthermore, our method may also find applications in the development of novel OA screening and/or rehabilitation programs, or translate to other domains. We believe that our work makes a significant step in accelerating the market introduction of OA DMOADs. To advance further development of AS in OA, all our codes are made publicly available at <https://github.com/Oulu-IMEDS/OACostSensitivityRL>.

References

- Ahmad, S., Yu, A.J., 2013. Active sensing as bayes-optimal sequential decision making. *arXiv preprint arXiv:1305.6650*.
- Ahuja, K., Zame, W., van der Schaar, M., 2017. Dpscreen: Dynamic personalized screening. *Advances in Neural Information Processing Systems* 30.
- Alaa, A.M., Van Der Schaar, M., 2016. Balancing suspense and surprise: Timely decision making with endogenous information acquisition. *Advances in Neural Information Processing Systems* 29.
- Altman, R.D., Gold, G., 2007. Atlas of individual radiographic features in osteoarthritis, revised. *Osteoarthritis and cartilage* 15, A1–A56.
- Anas, I., Musa, T.A., Kabiru, I., Yisau, A.A., Kazaure, I.S., Abba, S.M., Kabir, S.M., 2013. Digital radiographic measurement of normal knee joint space in adults at kano, nigeria. *The Egyptian Journal of Radiology and Nuclear Medicine* 44, 253–258.
- Bellamy, N., Buchanan, W.W., Goldsmith, C.H., Campbell, J., Stitt, L.W., 1988. Validation study of womac: a health status instrument for measuring clinically important patient relevant outcomes to antirheumatic drug therapy in patients with osteoarthritis of the hip or knee. *The Journal of rheumatology* 15, 1833–1840.
- Berkson, J., 1944. Application of the logistic function to bio-assay. *Journal of the American statistical association* 39, 357–365.
- Bourne, R.B., Chesworth, B.M., Davis, A.M., Mahomed, N.N., Charron, K.D., 2010. Patient satisfaction after total knee arthroplasty: who is satisfied and who is not? *Clinical Orthopaedics and Related Research* 468, 57–63.
- Buckland-Wright, J.C., Macfarlane, D.G., Lynch, J.A., Jasani, M.K., Bradshaw, C.R., 1995. Joint space width measures cartilage thickness in osteoarthritis of the knee: high resolution plain film and double contrast macro-radiographic investigation. *Annals of the rheumatic diseases* 54, 263–268.
- Chang, C.H., Mai, M., Goldenberg, A., 2019. Dynamic measurement scheduling for event forecasting using deep rl, in: *International Conference on Machine Learning*, PMLR. pp. 951–960.
- Cho, Y., Jeong, S., Kim, H., Kang, D., Lee, J., Kang, S.B., Kim, J.H., 2021. Disease-modifying therapeutic strategies in osteoarthritis: Current status and future directions. *Experimental & molecular medicine* 53, 1689–1696.
- Chung, J., Gulcehre, C., Cho, K., Bengio, Y., 2014. Empirical evaluation of gated recurrent neural networks on sequence modeling. *arXiv preprint arXiv:1412.3555*.
- Cigdem, O., Deniz, C.M., 2023. Artificial intelligence in knee osteoarthritis: A comprehensive review. *Osteoarthritis Imaging*, 100161.
- Contartese, D., Tschon, M., De Mattei, M., Fini, M., 2020. Sex specific determinants in osteoarthritis: a systematic review of preclinical studies. *International journal of molecular sciences* 21, 3696.
- Cox, D.R., 1972. Regression models and life-tables. *Journal of the Royal Statistical Society: Series B (Methodological)* 34, 187–202.
- Cuzick, J., 2023. The importance of long-term follow up of participants in clinical trials. *British journal of cancer* 128, 432–438.
- Driban, J.B., Harkey, M.S., Barbe, M.F., Ward, R.J., MacKay, J.W., Davis, J.E., Lu, B., Price, L.L., Eaton, C.B., Lo, G.H., et al., 2020. Risk factors and the natural history of accelerated knee osteoarthritis: a narrative review. *BMC musculoskeletal disorders* 21, 1–11.
- Duryea, J., Neumann, G., Niu, J., Totterman, S., Tamez, J., Dabrowski, C., Le Graverand, M.P.H., Luchi, M., Beals, C.R., Hunter, D.J., 2010. Comparison of radiographic joint space width with magnetic resonance imaging cartilage morphometry: analysis of longitudinal data from the osteoarthritis initiative. *Arthritis care & research* 62, 932–937.
- Eckstein, F., Collins, J., Nevitt, M., Lynch, J., Kraus, V., Katz, J., Losina, E., Wirth, W., Guermazi, A., Roemer, F., et al., 2015. Cartilage thickness change as an imaging biomarker of knee osteoarthritis progression—data from the fhni oa biomarkers consortium. *Arthritis & rheumatology (Hoboken, NJ)* 67, 3184.
- Evans, M., 2018. What does knee surgery cost? few know, and that's a problem. *Wall Street Journal* 21.
- Eymard, F., Parsons, C., Edwards, M., Petit-Dop, F., Reginster, J.Y., Bruyère, O., Richette, P., Cooper, C., Chevalier, X., 2015. Diabetes is a risk factor for knee osteoarthritis progression. *Osteoarthritis and cartilage* 23, 851–859.
- Gandhi, N., Qadeer, A.S., Meher, A., Rachel, J., Patra, A., John, J., Anilkumar, A., Dutta, A., Nanda, L., Rout, S.K., 2023. Costs and models used in the economic analysis of total knee replacement (tkr): A systematic review. *Plos one* 18, e0280371.
- Guan, B., Liu, F., Haj-Mirzaian, A., Demehri, S., Samsonov, A., Neogi, T., Guermazi, A., Kijowski, R., 2020. Deep learning risk assessment models for predicting progression of radiographic medial joint space loss over a 48-month follow-up period. *Osteoarthritis and cartilage* 28, 428–437.
- Hafez, A.R., Alenazi, A.M., Kachanathu, S.J., Alroumi, A., Mohamed, E., et al., 2014. Knee osteoarthritis: a review of literature. *Phys Med Rehabil Int* 1, 8.
- Hallaj, E., Le, Y., Hicks, J.L., Hastie, T.J., Delp, S.L., 2018. Modeling and predicting osteoarthritis progression: data from the osteoarthritis initiative. *Osteoarthritis and cartilage* 26, 1643–1650.
- Hirsch, J.A., Leslie-Mazwi, T.M., Nicola, G.N., Barr, R.M., Bello, J.A., Donovan, W.D., Tu, R., Alson, M.D., Manchikanti, L., 2015. Current procedural terminology; a primer. *Journal of neurointerventional surgery* 7, 309–312.
- Hirvasniemi, J., Runhaar, J., van der Heijden, R., Zokaeinikoo, M., Yang, M., Li, X., Tan, J., Rajamohan, H., Zhou, Y., Deniz, C., et al., 2023. The knee osteoarthritis prediction (knoap2020) challenge: An image analysis challenge to predict incident symptomatic radiographic knee osteoarthritis from mri and x-ray images. *Osteoarthritis and Cartilage* 31, 115–125.
- Hochreiter, S., Schmidhuber, J., 1997. Long short-term memory. *Neural computation* 9, 1735–1780.
- Holt, S., Hüyük, A., van der Schaar, M., 2024. Active observing in continuous-time control. *Advances in Neural Information Processing Systems* 36.
- Hu, K., Wu, W., Li, W., Simic, M., Zomaya, A., Wang, Z., 2022. Adversarial evolving neural network for longitudinal knee osteoarthritis prediction. *IEEE Transactions on Medical Imaging* 41, 3207–3217.
- Hunter, D.J., 2011. Pharmacologic therapy for osteoarthritis—the era of disease modification. *Nature Reviews Rheumatology* 7, 13–22.
- Jamshidi, A., Pelletier, J.P., Labbe, A., Abram, F., Martel-Pelletier, J., Droit, A., 2021. Machine learning-based individualized survival prediction model

- for total knee replacement in osteoarthritis: data from the osteoarthritis initiative. *Arthritis care & research* 73, 1518–1527.
- Jarrett, D., Van Der Schaar, M., 2020. Inverse active sensing: Modeling and understanding timely decision-making. *arXiv preprint arXiv:2006.14141*.
- Joo, P.Y., Borjali, A., Chen, A.F., Muratoglu, O.K., Varadarajan, K.M., 2022. Defining and predicting radiographic knee osteoarthritis progression: a systematic review of findings from the osteoarthritis initiative. *Knee Surgery, Sports Traumatology, Arthroscopy* 30, 4015–4028.
- Karita, S., Chen, N., Hayashi, T., Hori, T., Inaguma, H., Jiang, Z., Someki, M., Soplin, N.E.Y., Yamamoto, R., Wang, X., et al., 2019. A comparative study on transformer vs rnn in speech applications, in: 2019 IEEE Automatic Speech Recognition and Understanding Workshop (ASRU), IEEE. pp. 449–456.
- Kellgren, J.H., Lawrence, J., 1957. Radiological assessment of osteo-arthrosis. *Annals of the rheumatic diseases* 16, 494.
- Kingma, D.P., Ba, J., 2014. Adam: A method for stochastic optimization. URL: <https://arxiv.org/abs/1412.6980>, *arXiv:1412.6980*.
- Kjellberg, J., Kehlet, H., 2016. A nationwide analysis of socioeconomic outcomes after hip and knee replacement. *Dan Med J* 63, A5257.
- Kollias, D., Tagaris, A., Stafylopatis, A., Kollias, S., Tagaris, G., 2018. Deep neural architectures for prediction in healthcare. *Complex & Intelligent Systems* 4, 119–131.
- Latourte, A., Kloppenburg, M., Richette, P., 2020. Emerging pharmaceutical therapies for osteoarthritis. *Nature Reviews Rheumatology* 16, 673–688.
- Lee, C., Yoon, J., Van Der Schaar, M., 2019. Dynamic-deephit: A deep learning approach for dynamic survival analysis with competing risks based on longitudinal data. *IEEE Transactions on Biomedical Engineering* 67, 122–133.
- Lee, J.M., Hauskrecht, M., 2023. Personalized event prediction for electronic health records. *Artificial Intelligence in Medicine* 143, 102620.
- Leung, K., Zhang, B., Tan, J., Shen, Y., Geras, K.J., Babb, J.S., Cho, K., Chang, G., Deniz, C.M., 2020. Prediction of total knee replacement and diagnosis of osteoarthritis by using deep learning on knee radiographs: data from the osteoarthritis initiative. *Radiology* 296, 584–593.
- Marsh, J., Joshi, I., Somerville, L., Vasarhelyi, E., Lanting, B., 2022. Health care costs after total knee arthroplasty for satisfied and dissatisfied patients. *Canadian Journal of Surgery* 65, E562.
- McAlindon, T., Cooper, C., Kirwan, J., Dieppe, P., 1993. Determinants of disability in osteoarthritis of the knee. *Annals of the rheumatic diseases* 52, 258–262.
- McCabe, P.G., Lisboa, P., Baltzopoulos, B., Olier, I., 2022. Externally validated models for first diagnosis and risk of progression of knee osteoarthritis. *PLoS one* 17, e0270652.
- Mnih, V., Kavukcuoglu, K., Silver, D., Graves, A., Antonoglou, I., Wierstra, D., Riedmiller, M., 2013. Playing atari with deep reinforcement learning. *arXiv preprint arXiv:1312.5602*.
- Mnih, V., Kavukcuoglu, K., Silver, D., Rusu, A.A., Veness, J., Bellemare, M.G., Graves, A., Riedmiller, M., Fidjeland, A.K., Ostrovski, G., et al., 2015. Human-level control through deep reinforcement learning. *nature* 518, 529–533.
- Nguyen, H.H., Blaschko, M.B., Saarakkala, S., Tiulpin, A., 2023. Clinically-inspired multi-agent transformers for disease trajectory forecasting from multimodal data. *IEEE Transactions on Medical Imaging*.
- Nguyen, H.H., Saarakkala, S., Blaschko, M.B., Tiulpin, A., 2020. Semixup: in-and-out-of-manifold regularization for deep semi-supervised knee osteoarthritis severity grading from plain radiographs. *IEEE Transactions on Medical Imaging* 39, 4346–4356.
- Nguyen, H.H., Saarakkala, S., Blaschko, M.B., Tiulpin, A., 2022. Clima: Clinically-inspired multi-agent transformers for knee osteoarthritis trajectory forecasting, in: 2022 IEEE 19th International Symposium on Biomedical Imaging (ISBI), IEEE. pp. 1–5.
- Oo, W.M., Yu, S.P.C., Daniel, M.S., Hunter, D.J., 2018. Disease-modifying drugs in osteoarthritis: current understanding and future therapeutics. *Expert opinion on emerging drugs* 23, 331–347.
- Pan, Q., O'Connor, M.I., Coutts, R.D., Hyzy, S.L., Olivares-Navarrete, R., Schwartz, Z., Boyan, B.D., 2016. Characterization of osteoarthritic human knees indicates potential sex differences. *Biology of sex differences* 7, 1–15.
- Panfilov, E., Saarakkala, S., Nieminen, M.T., Tiulpin, A., 2022. Predicting knee osteoarthritis progression from structural mri using deep learning, in: 2022 IEEE 19th International Symposium on Biomedical Imaging (ISBI), IEEE. pp. 1–5.
- Panfilov, E., Saarakkala, S., Nieminen, M.T., Tiulpin, A., 2023. End-to-end prediction of knee osteoarthritis progression with multi-modal transformers. *arXiv preprint arXiv:2307.00873*.
- Pei, H., Yang, B., Liu, J., Dong, L., 2018. Group sparse bayesian learning for active surveillance on epidemic dynamics, in: *Proceedings of the AAAI Conference on Artificial Intelligence*.
- Pfrizer, 2010. A long-term, placebo-controlled x-ray study investigating the safety and efficacy of sd-6010 in subjects with osteoarthritis of the knee (itic). <https://classic.clinicaltrials.gov/ct2/show/NCT00565812>.
- Pham, T., Tran, T., Phung, D., Venkatesh, S., 2017. Predicting healthcare trajectories from medical records: A deep learning approach. *Journal of biomedical informatics* 69, 218–229.
- Phillips, J.L., Rondon, A.J., Vannello, C., Fillingham, Y.A., Austin, M.S., Courtney, P.M., 2019. How much does a readmission cost the bundle following primary hip and knee arthroplasty? *The Journal of Arthroplasty* 34, 819–823.
- Price, A.J., Alvand, A., Troelsen, A., Katz, J.N., Hooper, G., Gray, A., Carr, A., Beard, D., 2018. Knee replacement. *The Lancet* 392, 1672–1682.
- Primorac, D., Molnar, V., Rod, E., Jeleč, Ž., Čukelj, F., Matišič, V., Vrdoljak, T., Hudetz, D., Hajsok, H., Borič, I., 2020. Knee osteoarthritis: a review of pathogenesis and state-of-the-art non-operative therapeutic considerations. *Genes* 11, 854.
- Qin, Y., van der Schaar, M., Lee, C., 2024. Risk-averse active sensing for timely outcome prediction under cost pressure. *Advances in Neural Information Processing Systems* 36.
- Ratzlaff, C., Ashbeck, E.L., Guermazi, A., Roemer, F.W., Duryea, J., Kwok, C.K., 2018. A quantitative metric for knee osteoarthritis: reference values of joint space loss. *Osteoarthritis and cartilage* 26, 1215–1224.
- Reddy, B.K., Delen, D., 2018. Predicting hospital readmission for lupus patients: An rnn-lstm-based deep-learning methodology. *Computers in biology and medicine* 101, 199–209.
- Rodriguez-Merchan, E.C., 2023. The current role of disease-modifying osteoarthritis drugs. *Archives of Bone and Joint Surgery* 11, 11.
- Roemer, F.W., Eckstein, F., Hayashi, D., Guermazi, A., 2014. The role of imaging in osteoarthritis. *Best practice & research Clinical rheumatology* 28, 31–60.
- Roemer, F.W., Guermazi, A., Demehri, S., Wirth, W., Kijowski, R., 2022. Imaging in osteoarthritis. *Osteoarthritis and cartilage* 30, 913–934.
- Spreafico, A., Hansen, A.R., Abdul Razak, A.R., Bedard, P.L., Siu, L.L., 2021. The future of clinical trial design in oncology. *Cancer discovery* 11, 822–837.
- Sun, R., Giles, C.L., 2001. Sequence learning: From recognition and prediction to sequential decision making. *IEEE Intelligent Systems* 16, 67–70.
- Sutton, R.S., Barto, A.G., 2018. *Reinforcement learning: An introduction*. MIT press.
- Tanguay-Sabourin, C., Fillingim, M., Guglietti, G.V., Zare, A., Parisien, M., Norman, J., Sweatman, H., Da-Ano, R., Heikkala, E., 15, P.A.R.G.B.J.C...M.J.P.J...T.M.J., et al., 2023. A prognostic risk score for development and spread of chronic pain. *Nature Medicine* 29, 1821–1831.
- Tesauro, G., et al., 1995. Temporal difference learning and td-gammon. *Communications of the ACM* 38, 58–68.
- Thorwarth Jr, W.T., 2004. From concept to cpt code to compensation: how the payment system works. *Journal of the American College of Radiology* 1, 48–53.
- Tiulpin, A., Klein, S., Bierma-Zeinstra, S.M., Thevenot, J., Rahtu, E., Meurs, J.v., Oei, E.H., Saarakkala, S., 2019a. Multimodal machine learning-based knee osteoarthritis progression prediction from plain radiographs and clinical data. *Scientific reports* 9, 20038.
- Tiulpin, A., Melekhov, I., Saarakkala, S., 2019b. Kneel: Knee anatomical landmark localization using hourglass networks, in: *Proceedings of the IEEE/CVF International Conference on Computer Vision Workshops*, pp. 0–0.
- Tiulpin, A., Saarakkala, S., Mathiessen, A., Hammer, H.B., Furnes, O., Nordsetten, L., Englund, M., Magnusson, K., 2022. Predicting total knee arthroplasty from ultrasonography using machine learning. *Osteoarthritis and Cartilage Open* 4, 100319.
- Tolpadi, A.A., Lee, J.J., Pedroia, V., Majumdar, S., 2020. Deep learning predicts total knee replacement from magnetic resonance images. *Scientific reports* 10, 6371.
- Ware, J.E., Kosinski, M., Keller, S.D., 1996. A 12-item short-form health survey: construction of scales and preliminary tests of reliability and validity.

- Medical care 34, 220–233.
- Watkins, C.J., Dayan, P., 1992. Q-learning. *Machine learning* 8, 279–292.
- Wu, C.C., Suen, S.c., 2022. Optimizing diabetes screening frequencies for at-risk groups. *Health Care Management Science* 25, 1–23.
- Yala, A., Mikhael, P.G., Lehman, C., Lin, G., Strand, F., Wan, Y.L., Hughes, K., Satuluru, S., Kim, T., Banerjee, I., et al., 2022. Optimizing risk-based breast cancer screening policies with reinforcement learning. *Nature medicine* 28, 136–143.
- Yao, Q., Wu, X., Tao, C., Gong, W., Chen, M., Qu, M., Zhong, Y., He, T., Chen, S., Xiao, G., 2023. Osteoarthritis: pathogenic signaling pathways and therapeutic targets. *Signal transduction and targeted therapy* 8, 56.
- Yoon, J., Jordon, J., Schaar, M., 2019. Asac: Active sensing using actor-critic models, in: *Machine Learning for Healthcare Conference*, PMLR. pp. 451–473.
- Yu, S., Krishnapuram, B., Rosales, R., Rao, R.B., 2009. Active sensing, in: *Artificial Intelligence and Statistics*, PMLR. pp. 639–646.

Supplementary material

S1.1. Reference methods details

The policies used as the reference methods are described below.

- **Random.** Randomly chooses an action with different probabilities at every time point for every patient.
- **NS.** Dismissal/follow-up skip actions are taken to all subjects at all follow-up points.
- **Bi-annual sensing.** A policy that recommends following up on every subject every 2 years.
- **Annual sensing.** A policy that recommends following up on every subject annually.
- **LR** (Berkson, 1944). We generated all possible input states with the different time index combinations for the training set. The target is in a set of $\{0, 1\}$. We fit these unroll data to the LR model. By grid scanning the model parameters, the best LR policy was achieved. Next, we test the trained LR policy at each time point respectively, the input for the next time point is modified according to predictions, and the update rule follows Section 2.1.
- **Cox regression** (Cox) (Cox, 1972). A time-to-event method that allows to estimate when the progression event occurs. This method aims to detect the first KOA progression based on only the baseline data. Hence, after achieving the best model through grid searching parameters, to earn the multi-events predictions, we adjusted the way of testing the model. In testing, based on the predicted progression event, new inputs were updated, and we requested the model to continuously forecast the next event until the prediction exceeds the evaluated time T .
- **GRU** (Chung et al., 2014) **and LSTM** (Hochreiter and Schmidhuber, 1997). RNN-based methods to estimate a sequence from input. We implemented dynamic learning into both GRU and LSTM. Dynamic learning allows us to make predictions based on the data in the latest

visit. We applied an action-dependent mask for every input state during the training process of GRU and LSTM. The combination of the new input state and the hidden state from the previous step was implemented into models to estimate the next action.

- **Dynamic-DeepHit** (DeepHit) (Lee et al., 2019) incorporates the longitudinal data and learns the time-to-event distributions by utilizing DL, aiming to update survival predictions dynamically. DeepHit proposed 2 subnetworks: a shared subnetwork to learn the history of measurements; and a cause-specific subnetwork to capture the risk for each competing event. The former network consists of an RNN structure and an attention mechanism, while the latter one is composed of fully-connected layers. This method dynamically updated the risk of progression when new data recorded. We implemented their published repository with paper and prepared unrolled data for the training process.

S1.2. Data behind figures

Table S1: Balanced accuracy and recall scores (mean and standard error, %) of our method and CLIMAT performed with knee-level and patient-level settings, presented at each year. Bold numbers represent the highest scores among all methods.

	Method	Year(s)	BA(%)	RC(%)
Knee-level	CLIMATv2	1	57.09 ± 1.69	24.29 ± 6.22
		2	50.87 ± 1.26	23.77 ± 4.30
		3	56.34 ± 0.84	46.15 ± 5.00
		4	55.60 ± 1.16	38.59 ± 4.55
	Ours	1	60.43 ± 0.72	58.98 ± 3.84
		2	59.26 ± 0.57	82.92 ± 1.83
		3	47.30 ± 0.80	32.88 ± 0.72
		4	59.41 ± 0.73	38.51 ± 1.95
Patient-level	CLIMATv2	1	51.83 ± 0.77	7.55 ± 3.18
		2	56.71 ± 0.95	42.83 ± 5.97
		3	58.73 ± 0.79	50.58 ± 3.24
		4	58.38 ± 0.89	50.16 ± 4.80
	Ours	1	62.81 ± 0.57	74.08 ± 2.62
		2	53.56 ± 0.44	96.98 ± 0.85
		3	60.40 ± 0.67	67.69 ± 1.03
		4	64.55 ± 0.74	55.94 ± 1.56

Table S2: RPP achieved by baselines and our policy from various cost settings, where (a) adjusting follow-up cost λ while keeping constant MLAC $c = 2$, (b) hold $\lambda = 0.5$ while varying c , (c) performance of our policy on grid combination between λ and c .

(a) With $c = 2$, varying λ

λ	NS	ANS	CLIMATv2	Ours
0.00	-1.64	1.14	-0.51	1.18
0.25	-1.64	-0.06	-0.74	0.54
0.50	-1.64	-0.86	-0.89	0.34
0.75	-1.64	-2.06	-1.12	-0.23
1.00	-1.64	-2.86	-1.27	-0.69
1.50	-1.64	-4.86	-1.65	-1.10
2.00	-1.64	-6.86	-2.03	-1.16

(b) With $\lambda = 0.5$, varying c

c	NS	ANS	CLIMATv2	Ours
0.50	-0.41	-1.71	-0.51	-0.36
1.00	-0.82	-1.43	-0.63	-0.35
1.50	-1.23	-1.15	-0.76	-0.05
2.00	-1.64	-0.87	-0.89	0.34

(c) RPP gained by our RL policy depending on c and λ combinations. Underscored numbers indicate positive or close to 0 RPP values.

λ	c					
	0.50	1.00	1.50	2.00	3.00	4.00
0.00	<u>0.31</u>	<u>0.61</u>	<u>0.92</u>	<u>1.18</u>	<u>1.85</u>	<u>2.45</u>
0.25	-0.14	<u>0.15</u>	<u>0.36</u>	<u>0.54</u>	<u>1.19</u>	<u>1.83</u>
0.50	-0.36	-0.36	<u>-0.05</u>	<u>0.34</u>	<u>0.65</u>	<u>1.20</u>
0.75	-0.44	-0.54	-0.48	-0.23	<u>0.16</u>	<u>0.71</u>
1.00	-0.49	-0.65	-0.75	-0.69	<u>-0.09</u>	<u>0.16</u>
1.50	-0.45	-0.83	-0.97	-1.10	-1.01	-0.52
2.00	-0.42	-0.90	-1.16	-1.16	-1.49	-1.35
2.50	-0.41	-0.85	-1.31	-1.45	-1.61	-1.85
3.00	-0.41	-0.85	-1.22	-1.75	-1.68	-2.09
3.50	-0.41	-0.83	-1.21	-1.78	-2.01	-2.18
4.00	-0.41	-0.82	-1.28	-1.78	-2.22	-2.33

Table S3: Number of visits (mean and standard error) of 3 policies according to pairs of KLGs at baseline. Those policies were trained with different follow-up costs hyper-parameter $\lambda = \{0.5, 0.8, 1.0\}$.

Baseline KLGs	Policies		
	$\lambda = 0.5$	$\lambda = 0.8$	$\lambda = 1.0$
(0, 0)	1.33 ± 0.18	1.07 ± 0.10	1.03 ± 0.06
(0, 1)	1.34 ± 0.20	1.13 ± 0.11	1.04 ± 0.07
(1, 1)	1.65 ± 0.29	1.31 ± 0.22	1.14 ± 0.13
(0, 2)	1.94 ± 0.32	1.46 ± 0.26	1.18 ± 0.15
(1, 2)	2.01 ± 0.33	1.52 ± 0.23	1.31 ± 0.18
(2, 2)	2.06 ± 0.33	1.59 ± 0.24	1.25 ± 0.16
(0, 3)	3.03 ± 0.31	2.31 ± 0.30	1.51 ± 0.20
(1, 3)	2.83 ± 0.32	2.20 ± 0.30	1.53 ± 0.20
(2, 3)	2.96 ± 0.32	2.16 ± 0.29	1.76 ± 0.26
(3, 3)	3.61 ± 0.21	2.88 ± 0.28	2.15 ± 0.25
(1, 4)	3.83 ± 0.12	3.30 ± 0.23	2.02 ± 0.21
(2, 4)	3.38 ± 0.17	2.88 ± 0.25	2.28 ± 0.23
(3, 4)	3.96 ± 0.06	3.24 ± 0.28	2.24 ± 0.27